Int. J. Electrochem. Sci., 8 **(2013)** 3721 - 3730

International Journal of
ELECTROCHEMICAL
SCIENCE
www.electrochemsci.org

Investigation of Enhanced Photoelectrochemical Property of Cerium Doped Hematite Film Prepared by Sol-Gel Route

Xin Yang[1,2], *Xiaojuan Lian*[1,2], *Shangjun Liu*[1], *Jing Tian*[1], *Chunping Jiang*[1], *Gang Wang*[1], *Jinwei Chen*[1] *and Ruilin Wang*[1,*]

[1] College of Materials Science and Engineering, Sichuan University, 610065, Chengdu, China
[2] Chongqing Key Laboratory of Micro/Nano Materials Engineering and Technology, Chongqing University of Arts and Sciences, 402160, Chongqing, China
[*]E-mail: rlwang26@yahoo.com.cn

Received: 17 January 2013 / *Accepted:* 11 February 2013 / *Published:* 1 March 2013

Cerium doped iron oxide thin film was successfully prepared by sol-gel route. Their physical properties were characterized by X-ray diffraction (XRD), scanning electron microscope (SEM), X-ray photoelectron spectra (XPS) and UV-visible absorbance spectra. Ce doped Fe_2O_3 films exhibit features of hematite crystallographic phase from XRD results. Particles on the surface are wormlike after heat treatment from the morphology analysis. The incident photon to electron conversion efficiency (IPCE) of Ce doped hematite is 14% (400nm) at 0.4V vs. NHE, which is higher than the undoped hematite film. Cerium in hematite lattice could improve the conductivity of the thin film. Therefore the photo generated carriers could live longer rather than recombining with each other rapidly as in the undoped hematite. The estimated surface carrier concentrations N_d are about 1.2×10^{19} cm^{-3} and 8.1×10^{18} cm^{-3} for Ce doped and undoped films, respectively. Higher N_d could also contribute to better PEC performance.

Keywords: Hematite film; Doping; Photo-electrochemical performance; Mott-Schottky plot; IPCE

1. INTRODUCTION

Hydrogen is an ideal renewable energy source, which can be reduced from water splitting by solar energy. By far, many materials have been studied as photo catalysts for water oxidation in decades. However, due to all kinds of defects of the materials, such as mismatch of energy gap and photo corrosion of the material, etc, no suitable photo catalysts have been developed. α-Fe_2O_3, as an n-

type metal oxide semiconductor, has the potential to be an economical photo catalyst because of its narrow band gap, low cost and vast storage [1]. Different kinds of methods were used to prepare high photo active α-Fe_2O_3 photo anodes and the incident photon to electron conversion efficiency (IPCE) of thin film anodes varied with the preparation routes. In order to increase the conversion efficiency, impurity doping is a convenient way to improve the photocatalytic performance. One way of that is donor doping, such Ti^{4+}, Sn^{4+}, Si^{4+}, etc. So far, the highest IPCE of α-Fe_2O_3 photo anode was obtained from the surface cobalt modified Si-doped polycrystalline hematite prepared by APCVD (IPCE=36% at 400 nm and 1.23 V vs. RHE) [2]. Dendritic nanostructure and SiO_2 interlayer both contributed to that unprecedented efficiency. Ti-doped hematite anode prepared by reactive sputtering [3] showed IPCE=15% at 400nm and 0.5V vs. SCE, which was higher than the undoped hematite anode. 4 atom % Sn-doped anode deposited by reactive ballistic [4] deposition showed IPCE=23% at 400nm at 1.4V vs. RHE, because the each Sn^{4+} ion could contribute one free electron and the conductivity and life of carrier were both improved. Undoped hematite anode deposited by ultra sonic pyrolysis (USP) method also exhibited high photo activity (IPCE=23% at 400nm and 1.42 V vs. RHE) [5]. The Ti-doped wormlike hematite film fabricated by sol-gel route showed obviously increase in the IPCE measurement (IPCE=32%, 0V vs. SCE) [6]. Some other elements, e.g. Cr [7, 8], Mo [7, 8], were also investigated. The second way of doping is acceptor doping, such Mg^{2+} [9], Zn^{2+} [10, 11], Cu^{2+} [11, 12], Ag^{+} [13], etc, which could change the intrinsic n-type into p-type. But the results were not as well as the donor doping by now. Sol-gel spin coating is an effective and convenient way to dope elements in the research target. As mentioned above, the doping impurities are mostly transition metals and there are few researches on the rare earth metal doping. CeO_2 is a direct band gap semiconductor with E_g=3.4eV [14] with well electro catalysis ability. It was commonly used as the CO oxidation catalyst in the vehicles exhaust [15]. Recently CeO_2 itself had been proved showing certain photo activity [16-18]. The Ce doped TiO_2 [19] showed increased activity in photo degradation of rhodamine B, and the CeO_2/$BiVO_4$ [20] composite photocatalyst exhibited enhanced photo degradation ability of methyl blue than each component alone.

However, the photoelectrochemical (PEC) property of Ce doped hematite film has not been investigated by others as far as we know. In this paper, the chemical state Ce in Fe_2O_3 film is established by XPS analysis. Photoelectrochemical properties of Ce doped hematite film are significantly changed compared with undoped hematite under the same condition.

2. EXPERIMENT

2.1 preparations of samples

All chemicals were used as received without further purification. Hydrate ferric nitrate $Fe(NO_3)_3 \cdot 9H_2O$ (99.99%) was dissolved in a mixture of acetyl acetone (≥99%), ethanol and polyvinylpyrrolidone and then stirred for 1h at the room temperature. After that certain amount of

$Ce(NO_3)_3 \cdot 6H_2O$ was added into the mixture and then the precursor was aged for 24 hours. Hematite films were prepared on fluorine-doped SnO_2 conducting glass substrates (FTO, 2.5cm×2.5cm) by spin coating method. The heat treatment was carried out in a tube furnace at 500°C for 2 hours.

2.2 physical characterizations

XRD was used to characterize the phase in a scanning range of 20-70° (2θ) with a rate of 0.02° per second (Cu $K\alpha_1$ radiation, λ=1.54056Å, 40kV, 25mA). The surface morphology was characterized by Hitachi S-4800 scanning electron microscope. X-ray photoelectron spectrum was carried out with Al Kα radiation source and the overall resolution was 0.1eV. UV-Visible absorbance spectrum was measured to study the light harvesting ability, and clean blank FTO glass was used as the standard baseline.

2.3 photoelectrochemical characterizations

The IPCE measurements were carried out in a self-made three arm cell fitted by a quartz window in 0.5M Na_2SO_4 solution. The system was made of an SBP500 monochromator, a Princeton scanning potentiostat, a Stanford Lock-in Amplifier, a calibrated Si dioxide and a 150W Xeon Lamp. The graphite rod was used as the counter electrode and Ag/AgCl (saturated KCl solution) as the reference electrode in all experiments. The potential conversion relationship between NHE and Ag/AgCl reference electrode is: $E_{NHE} = E_{Ag/AgCl} + 0.197V$ (25°C). Mott-Schottky plot were measured by Ametek Solartron 1287 impedance analyzer and 1260 electrochemical interface in 0.5M Na_2SO_4 solution with the frequency of 1000Hz.

3. RESULTS AND DISCUSSIONS

3.1 physical properties and characterizations

X-ray diffract meter was used to yield the crystal structure information and phase identification of films. The thickness measured by step profiler is about 60nm for both Ce doped film and undoped film. The main peaks are from the FTO layer, while the diffraction intensity of α-Fe_2O_3 peaks is weak. Figure 1a shows that both undoped and Ce doped films exhibit α phase of Fe_2O_3 (JCPDS card No. 330664) after annealing. The (104) peak is partially covered by (101) peak of FTO substrate， nevertheless the major peaks characteristic of α-Fe_2O_3 can be distinguished. There are no characteristic peaks of CeO_2 or Ce_2O_3 in the Ce doped film. The ion radius of Fe^{3+} is 0.64Å, while the ion radius of Ce^{4+} is 0.98 Å [21]. When Ce^{4+} ions are incorporated into α-Fe_2O_3 lattice, the lattice parameters could be slightly changed, which may cause α-Fe_2O_3 peaks shift. However, the position of characteristic

peaks do not shift after Ce doping, which means that Ce doping will not affect the lattice strongly or the sensitivity of the instrument is not enough to distinguish the difference [22].

Figure 1b shows SEM image of Ce doped hematite thin film. The film surface is composed of wormlike particles, which is in accordance with hematite film prepared by colloidal method [23]. The particle size of the Ce doped hematite film is between 35-130nm. With grooves among wormlike particles, the electrolyte could infiltrate into the bulk film easily. The contact area between electrolyte and film therefore is increased, which contributes to the carrier separation efficiency ultimately.

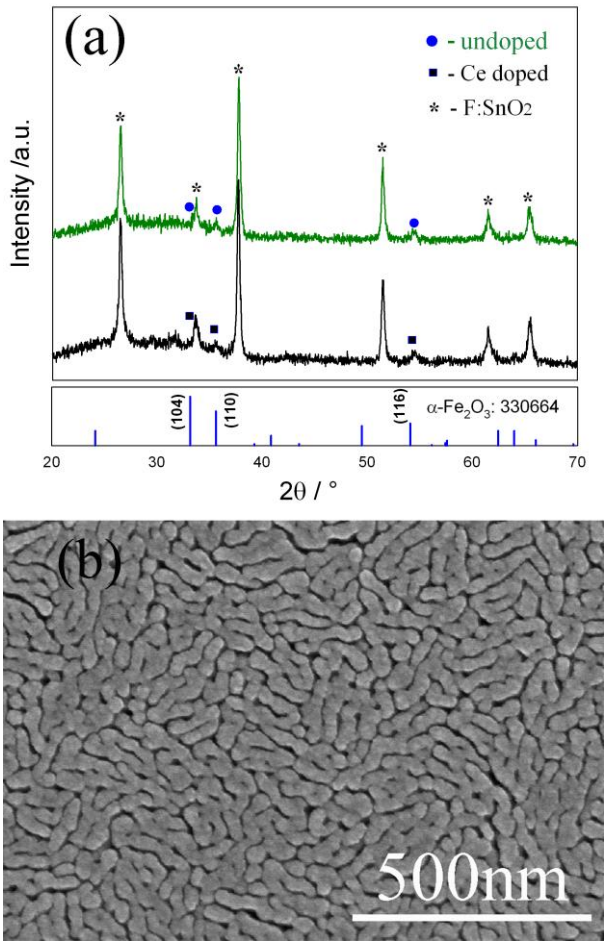

Figure 1. XRD patterns of undoped and Ce doped film (a); SEM image of Ce doped hematite film (b).

XPS was applied to study the surface chemical state of undoped and Ce doped hematite films. The analysis of XPS spectra was performed by high-resolution scans of the Fe 2p, O 1s and Ce 3d regions. As shown in figure 2a, Fe $2p_{3/2}$ peaks are located at a binding energy (BE) of 710.7 eV, and the Fe $2p_{1/2}$ peaks are located at a BE of 724.0 eV and 723.8eV for undoped hematite and Ce doped hematite samples, respectively (table 1). It is known that the oxidation state of the nonequivalent atom of the same element is increased with a higher binding energy peaks. This has been demonstrated by experimental values. Compared with the reported results of the Fe $2p_{3/2}$ peak (711.6 eV) and Fe $2p_{1/2}$

peak (725.1 eV) for α-Fe_2O_3 [24], it could be concluded that Fe $2p_{1/2}$ and Fe $2p_{3/2}$ peaks of two films are corresponding to Fe(III). The energy difference between Fe $2p_{3/2}$ and Fe $2p_{1/2}$ peaks is 14 eV. This value is characteristic of Fe^{3+} state indicating the formation of α-Fe_2O_3 by the experimental methodology [24, 25].

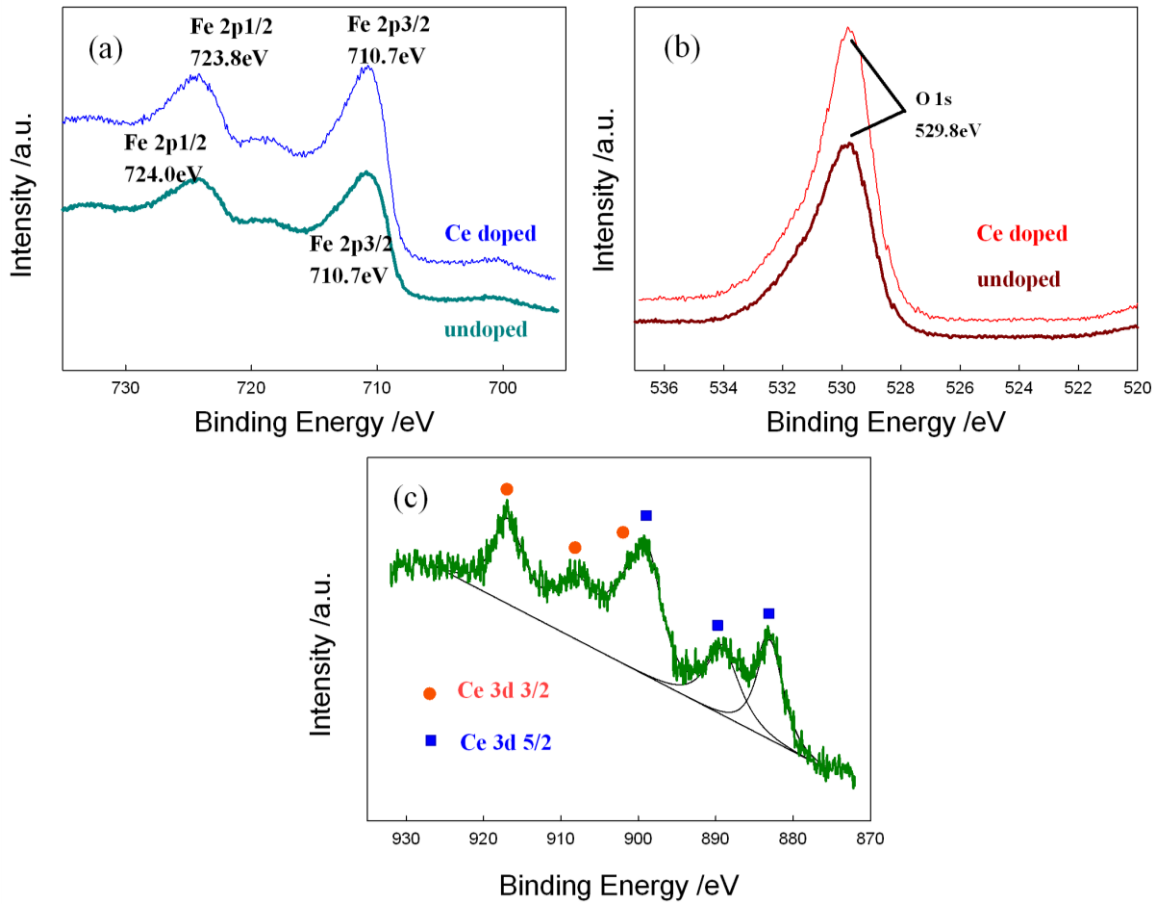

Figure 2. X-ray photoelectron spectroscopy studies of undoped and Ce doped hematite samples: (a) Fe 2p peaks, (b) O 1s peaks, heavy line for undoped hematite and thin line for Ce doped hematite; (c) Ce 3d peaks. Red circles for Ce $3d_{3/2}$ peaks and blue squares for Ce $3d_{5/2}$ peaks.

Table 1. XPS binding energies (BE) in eV for undoped and Ce doped hematite films.

Samples	Fe $2p_{3/2}$		Fe $2p_{1/2}$		O 1s
	BE±0.2	FWHM	BE±0.2	FWHM	BE±0.2
Undoped hematite	710.7	3.7	724.0	4.4	529.8
Ce doped hematite	710.7	3.6	723.8	4.5	529.8

Figure 2c shows that there are 6 peaks of the Ce 3d peaks. The Ce $3d_{3/2}$ peaks are located at BE of 916.7eV, 908.2eV and 902.0eV, and the Ce $3d_{5/2}$ peaks are located at BE of 898.8eV, 889.1eV and 883.0eV, respectively (table 2). All these characteristic peaks are corresponding to CeO_2 [26]. As a result, Ce atoms exists in the form of Ce(IV) state in the hematite lattice, which could donor one free electron in the hematite lattice. The slightly deviation of binding energy data may be induced by the mutual chemical reaction between Fe_2O_3 and CeO_2 [27, 28]. Ce^{4+} could donor one free electron in the hematite lattice, which will contribute to the electro conductivity of the film. From the integral area of Ce 3d peaks, the estimated mole content of cerium on the surface is 4.8%.

Table 2. XPS binding energies (BE) in eV of Ce 3d peaks.

Ce $3d_{3/2}$		Ce $3d_{5/2}$	
BE±0.2	FWHM	BE±0.2	FWHM
916.9	4.8	898.7	4.3
908.2	6.1	889.1	5.1
902.0	5.5	883.0	3.9

The undoped and Ce doped hematite films are orange-brown and semitransparent. The absorptions of undoped and Ce doped films are very similar. UV-visible absorbance spectra of each sample are shown in figure 3a. The deduction of energy gap is based on Tauc formula [29]:

$$(\alpha h\upsilon)^{1/2} \propto A\left(h\upsilon - E_g\right)$$

Here, the absorption coefficient, α is proportional to the square of photon energy in indirect transition condition. A is the proportionality constant, hν the photon energy and E_g the energy gap. Figure 3b shows that both films exhibit indirect transition gap, which is around 2.1eV. The indirect transition has been identified as Fe^{3+} 3d→3d excitation in the low photon energy scale, while the direct transition corresponds to the O^{2-} 2p→Fe^{3+} 3d charge transfer in the high photon energy area [5]. Instead of increasing, the absorbance of Ce doped film becomes smaller than the undoped hematite film in the short wavelength region. Because CeO_2 has a wide E_g=3.4eV [14], the optical band gap of Ce doped hematite film is a little wider than undoped hematite (figure 3b). Therefore, the absorption edge shifts slightly to the high photon energy direction.

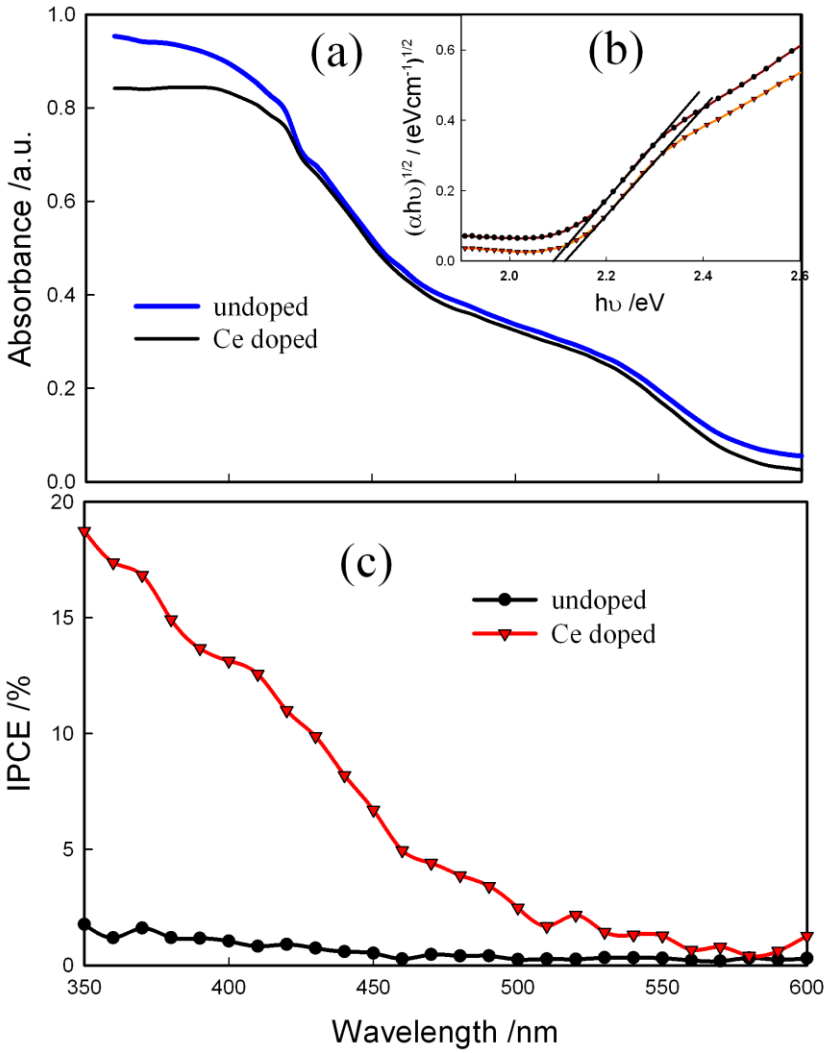

Figure 3. (a) UV-visible light absorbance of undoped and Ce doped hematite films; (b) indirect transition fit of energy gap, blank FTO as the baseline; (c) incident photon to electron conversion efficiency of undoped and Ce doped hematite films with bias of 0.4V vs. NHE in 0.5M Na_2SO_4, pH≈6.8.

3.2 IPCE and Mott-Schottky plot

The induced photon to electron conversion efficiency (IPCE) is defined as:

$$\mathrm{IPCE} = \frac{\mathrm{I}}{\mathrm{P}}\frac{1240}{\lambda} \times 100\%,$$

Here I is the photocurrent density ($mA \cdot cm^{-2}$), P is the power of monochromatic light irradiated on the electrode ($mW \cdot cm^{-2}$) and λ is the wavelength (nm). Figure 3c shows the IPCE measurements are

carried out under the bias of 0.4V vs. NHE. As expected, the IPCE of Ce doped sample is much higher than the IPCE of the undoped sample. Ce doped hematite shows the highest IPCE (19% at 350nm and 14% at 400nm), which is many times compared to the undoped film sample.

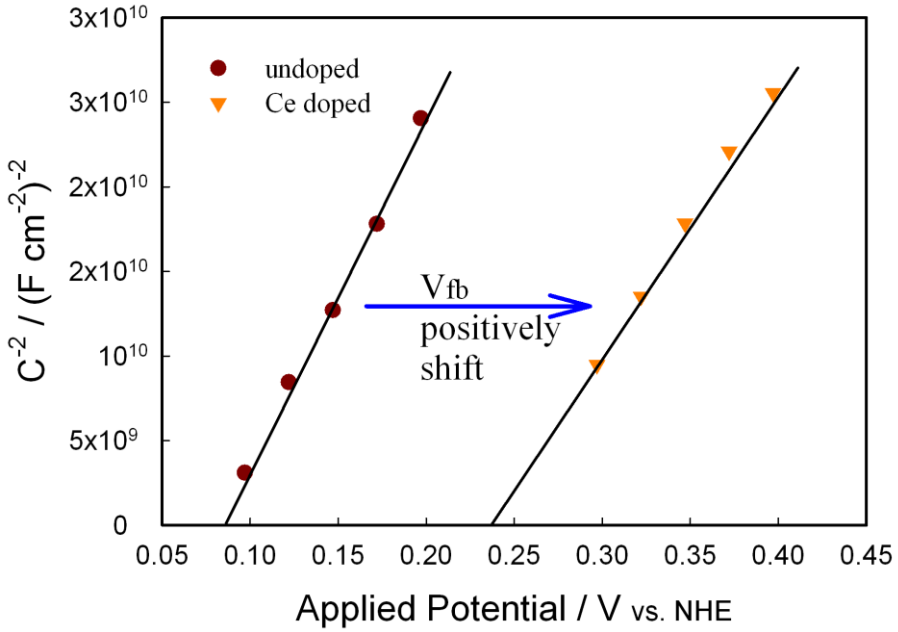

Figure 4. Mott-Schottky plots of undoped and Ce doped hematite films measured in 0.5M Na_2SO_4 with frequency of 1000Hz.

Assume that Fe is substituted by Ce in the hematite lattice [30, 31]. Ce^{4+} may play the role of electron donor and contribute one free electron in the hematite lattice as mentioned above. The bulk conductivity of the doped hematite may be improved than the undoped hematite by suppressing the charge recombination. Therefore when the photo generated carriers are the same in both Ce doped and undoped hematite films, Ce doped film anode could transfer electrons and holes more efficiently and perform a better photo current in the test.

The flat band potential V_{fb} can be determined from the Mott-Schottky plot. The equilibration of Femi level of α-Fe_2O_3 with the chemical potential of the electrolyte causes the flow of electrons to the α-Fe_2O_3/electrolyte interface, resulting in band bending in the near-surface region. The measurement is based on the theory of Schottky contact of α-Fe_2O_3/electrolyte interface. The capacitance is as function of electrochemical potential for an n-type semiconductor [32]:

$$\frac{1}{C_{sc}^2} = \frac{2}{e\varepsilon\varepsilon_0 N_d}(V - V_{fb} - \frac{k_B T}{e}).$$

Where C_{sc} is the capacity per unit area of space charge layer, e is the electron charge, ε is the dielectric constant of α-Fe_2O_3 ($\varepsilon_{\alpha\text{-}Fe2O3}$=80 [33]), ε_0 is the permittivity of vacuum, N_d is the carrier

concentration, V is the applied potential and V_{fb} is the flat band potential. The Mott-Schottky analysis is based on two assumptions. First, the electron donor should be fully ionized and homogeneously distributed in the space charge layer. Second, the electrode surface should be flat to the approximation of plate capacitance. Figure 4 shows that the V_{fb} of undoped and Ce doped hematite film are 0.08V and 0.24V vs. NHE, respectively. V_{fb} of Ce doped hematite film shifts positively about 0.16V, which is not good for the hydrogen evolution in the water splitting process compared with other reports [34]. But that does not affect the oxygen evolution process much. The estimated N_d of Ce doped and undoped hematite are about 1.2×10^{19} cm^{-3} and 8.1×10^{18} cm^{-3} respectively. With larger carrier concentration, Ce doped hematite film obtained better PEC performance.

4. CONCLUSIONS

Undoped and Ce doped hematite films were prepared in this study. From results of physical characterization, it is demonstrated that Ce has been doped into hematite film in the form of CeO_2. The crystallographic phase of Ce doped hematite film is not changed compared with undoped hematite film. Wormlike particles on the surface can increase the contact area between electrolyte and film and make the photo generated carriers live longer than that in undoped hematite film. Ce^{4+} in the bulk film can benefit the electro conductivity of hematite film and promote the charge transfer process. As a result, the recombination in the bulk and surface can be suppressed, which ultimately increase the PEC performance. In the Mott-Schottky test, the V_{fb} of Ce doped film shifts positively to 0.24V vs. NHE, which is not good for the hydrogen evolution. However, the IPCE of Ce doped hematite film is significantly improved from 3% to 19% at 350nm under 0.4V vs. NHE. Cerium, as a rare earth metal, has shown the potential in enhancing PEC properties of metal oxide.

ACKNOWLEDGEMENTS
This research is supported by 863 project (2006AA05Z102) and Specialized Research Fund for the Doctoral Program of Higher Education (20110181110003) and Chengdu Natural Science Foundation (10GGYB380-GX-023, 10GGYB828GX-023).

References

1. K. Sivula, F. Le Formal, M. Gratzel, *Chemsuschem*, 4 (2011) 432-449.
2. A. Kay, I. Cesar, M. Grätzel, *J. Am. Chem. Soc.*, 128 (2006) 15714-15721.
3. J.A. Glasscock, P.R.F. Barnes, I.C. Plumb, N. Savvides, *J. Phys. Chem. C*, 111 (2007) 16477-16488.
4. N.T. Hahn, H. Ye, D.W. Flaherty, A.J. Bard, C.B. Mullins, *ACS Nano*, 4 (2010) 1977-1986.
5. A. Duret, M. Grätzel, *J. Phys. Chem. B*, 109 (2005) 17184-17191.
6. X. Lian, X. Yang, S. Liu, Y. Xu, C. Jiang, J. Chen, R. Wang, *App. Sur. Sci.*, 258 (2012) 2307-2311.
7. P. Liao, J.A. Keith, E.A. Carter, *J. Am. Chem. Soc.*, 134 (2012) 13296-13309.

8. A. Kleiman-Shwarsctein, Y.-S. Hu, A.J. Forman, G.D. Stucky, E.W. McFarland, *J. Phys. Chem. C*, 112 (2008) 15900-15907.
9. Y. Lin, Y. Xu, M.T. Mayer, Z.I. Simpson, G. McMahon, S. Zhou, D. Wang, *J. Am. Chem. Soc.*, 134 (2012) 5508-5511.
10. W.B. Ingler, J.P. Baltrus, S.U.M. Khan, *J. Am. Chem. Soc.*, 126 (2004) 10238-10239.
11. V.R. Satsangi, S. Kumari, A.P. Singh, R. Shrivastav, S. Dass, *Int. J. Hydrogen Energ.*, 33 (2008) 312-318.
12. W.B. Ingler, S.U.M. Khan, *Int. J. Hydrogen Energ.*, 30 (2005) 821-827.
13. A. Watanabe, H. Kozuka, *J. Phys. Chem. B*, 107 (2003) 12713-12720.
14. J. Chen, D.Q. Meng, *Integr Ferroelectr*, 138 (2012) 145-151.
15. J. Qi, J. Chen, G. Li, S. Li, Y. Gao, Z. Tang, *Energ. Environ. Sci.*, 5 (2012) 8937-8941.
16. C. Karunakaran, P. Anilkumar, *Sol. Energ. Mat. Sol. C.*, 92 (2008) 490-494.
17. S.W. Bennett, A.A. Keller, *Appl. Catal. B-Environ.*, 102 (2011) 600-607.
18. C. Karunakaran, R. Dhanalakshmi, *Sol. Energ. Mat. Sol. C*, 92 (2008) 1315-1321.
19. M. He, D. Li, D. Jiang, M. Chen, *J. Solid State Chem.*, 192 (2012) 139-143.
20. N. Wetchakun, S. Chaiwichain, B. Inceesungyorn, K. Pingmuang, S. Phanichphant, A.I. Minett, J. Chen, *Acs. Appl. Mater. Inter.*, 4 (2012) 3718-3723.
21. R. Shannon, *Acta Crystallogr. A*, 32 (1976) 751-767.
22. L. Li, Y. Yang, X. Liu, R. Fan, Y. Shi, S. Li, L. Zhang, X. Fan, P. Tang, R. Xu, W. Zhang, Y. Wang, L. Ma, *App. Sur. Sci.*, 265 (2013) 36-40.
23. K. Sivula, R. Zboril, F. Le Formal, R. Robert, A. Weidenkaff, J. Tucek, J. Frydrych, M. Gratzel, *J. Am. Chem. Soc.*, 132 (2010) 7436-7444.
24. P. Mills, J.L. Sullivan, *J. Phys. D-Appl. Phys.*, 16 (1983) 723.
25. B.J. Tan, K.J. Klabunde, P.M.A. Sherwood, *Chem. Mater.*, 2 (1990) 186-191.
26. E. Paparazzo, G.M. Ingo, N. Zacchetti, *J Vac. Sci. Technol. A*, 9 (1991) 1416-1420.
27. R. López, R. Gómez, M.E. Llanos, *Catal. Today*, 148 (2009) 103-108.
28. N. Hellgren, M.P. Johansson, E. Broitman, L. Hultman, J.-E. Sundgren, *Phys. Rev. B*, 59 (1999) 5162-5169.
29. J. Tauc, *Science*, 158 (1967) 1543-1548.
30. H.G. Cha, J. Song, H.S. Kim, W. Shin, K.B. Yoon, Y.S. Kang, *Chem. Commun.*, 47 (2011) 2441-2443.
31. H. Magnan, D. Stanescu, M. Rioult, E. Fonda, A. Barbier, *Appl. Phy. Lett.*, 101 (2012) 133908-133904.
32. F. Cardon, W.P. Gomes, *J. Phys. D-Appl. Phys.*, 11 (1978) L63.
33. J.H. Kennedy, K.W. Frese, *J. Electrochem. Soc.*, 125 (1978) 723-726.
34. C.-Y. Chang, C.-H. Wang, C.-J. Tseng, K.-W. Cheng, L.-W. Hourng, B.-T. Tsai, *Int. J. Hydrogen Energ.*, 37 (2012) 13616-13622.